Research Inventy: International Journal of Engineering And Science
Vol.15, Issue 4 (April 2025), PP 35-40
Issn (e): 2278-4721, Issn (p):2319-6483, www.researchinventy.com

Experimental Determination of Thrust Force of Fixed-Pitch Propeller on Unmanned Aerial Vehicles

Bùi Văn Cường[1], Phan Đức Đình[1] and Nguyễn Thế Diện[1], Ngô Minh Tuấn[1], Bùi Đình Việt[1], Trần Phú Mạnh[1].
[1]*Air Defense – Air Force Academy, Viet Nam*
**Corresponding Author Email: Buivancuong.hv@gmail.com*

Abstract: *This paper presents research results on the dependence of thrust generated by fixed-pitch propellers on rotational speed and airflow velocity from a wind tunnel. Variations in propeller thrust due to changes in rotational speed and airflow velocity (flight speed) directly affect propeller efficiency. The experimental setup provides reliable data to establish propeller thrust characteristics during the design and operation phases of UAVs utilizing propellers in both civilian and military aviation.*

Keywords: *thrust, propeller, pitch angle, rotational speed, airflow velocity, aerodynamics.*

Date Of Submission: 24-04-2025 Date Of Acceptance: 03-05-2025

I. INTRODUCTION

Modern aerodynamic computational methods have advanced significantly; however, experimental testing in wind tunnels remains the predominant approach for determining the thrust characteristics of propellers. These experiments employ geometrically similar propeller models, utilizing specialized testing apparatus where the propeller is mounted within the working chamber of a wind tunnel. This paper presents research findings on the dependence of thrust generated by fixed-pitch propellers on two primary factors: the propeller's rotational speed and the airflow velocity in the wind tunnel. Tests were conducted under controlled aerodynamic conditions with varying rotational speeds and airflow velocities.

II. THEORETICAL BASIS

A propeller is a propulsion mechanism driven by a motor to generate rotational motion and produce thrust P. To determine the thrust generated by a rotating propeller that is moving axially at velocity V_0, consider a blade element at radius r with chord length b and thickness dr (Figure 1). When the propeller rotates at angular velocity Ω, the tangential velocity of the blade element is $U_0 = r\Omega$. Applying the reverse motion principle, assume an airflow with axial velocity V_0 and tangential velocity U_0 acts on a stationary blade element. The resultant airflow velocity relative to the blade element is the vector sum $\vec{W}_0 = \vec{V}_0 + \vec{U}_0$ defined as the relative velocity.

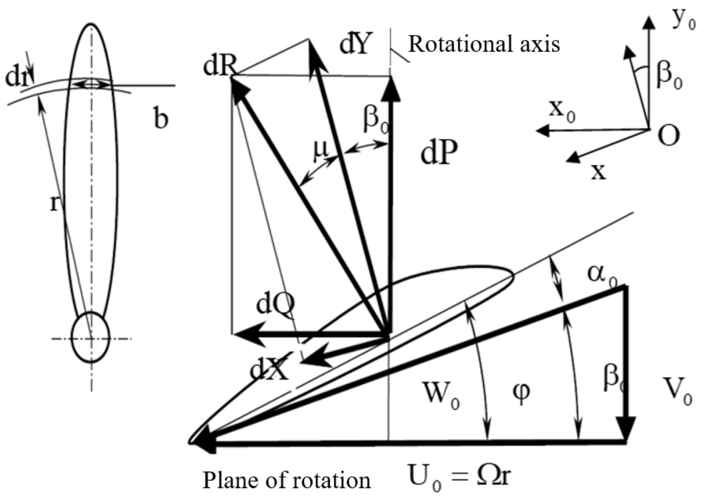

Figure 1. Characteristic Velocities and Forces Acting on a Blade Element

The vector $\vec{W}_0$ forms an angle of attack α_0 with the blade chord and an inflow angle β_0 with the rotational plane (Ox_0).

The relative advance ratio (or propeller velocity coefficient) is defined as:

$$\lambda = \frac{H_a}{d_{cq}} = \frac{V_0 \Delta t}{d_{cq}} = \frac{V_0}{n d_{cq}} = \frac{\pi V_0}{\Omega r_{cq}} = \pi \frac{V_0}{U_{0.cq}} = \pi \mathrm{tg}\beta_0$$

where: n: Rotational speed (revolutions per second), $n = 1/\Delta t = \Omega/(2\pi)$; H_a : Propeller advance per revolution, defined as the axial displacement of the propeller at velocity V_0 during one revolution Δt.

When airflow envelops a blade element, distributed aerodynamic loads combine to form dR – the total aerodynamic force acting on the element.

The projections of the total aerodynamic force dR onto the rotational axis (Oy_0) and the rotational plane (Ox_0) are the elemental thrust dP and elemental rotational drag dQ, respectively.

Alternatively, dR can be decomposed into components aligned with the velocity W_0 (Ox-axis) and perpendicular to W_0 (O*y*-axis), yielding the elemental drag force dX and elemental lift force dY. These forces are expressed using aerodynamic coefficients:

$$dX = C_x^{\alpha} \rho \frac{W_0^2}{2} b dr, \quad dY = C_y^{\alpha} \rho \frac{W_0^2}{2} b dr.$$

Integrating along the blade from the hub radius $\bar{r}_{ol}$ to the tip *r*=1, the total thrust P is derived as:

$$P = \rho n^2 d_{cq}^4 \frac{i\pi^2}{4} \int_{\bar{r}_{ol}}^{1} \frac{C_y^{\alpha} \cos\beta_0 - C_x^{\alpha} \sin\beta_0}{\cos^2\beta_0} \bar{b}\bar{r}^2 d\bar{r} \text{ or } P = \bar{\tau} \rho n^2 d_{cq}^4 .$$

where:

$$\bar{\tau} = \frac{i\pi^2}{4} \int_{\bar{r}_{ol}}^{1} \frac{C_y^{\alpha} \cos\beta_0 - C_x^{\alpha} \sin\beta_0}{\cos^2\beta_0} \bar{b}\bar{r}^2 d\bar{r} \text{ (termed the thrust coefficient)}$$

In the general case, the thrust coefficient τ depends on the inflow angle of the blade element β0 and the aerodynamic coefficients C_y^{α} and C_x^{α}. In other words, the propeller thrust P will depend on the relative advance ratio λ and the aerodynamic coefficients C_y^{α} and C_x^{α}. For a constant thrust coefficient (τ=const), P becomes a quadratic function of rotational speed (n), as illustrated in Figure 2.

For a fixed pitch angle ($\varphi = \text{const}$), an increase in the relative advance ratio ($\lambda\uparrow$) results in a higher inflow angle ($\beta_0\uparrow$). Consequently, the effective angle of attack decreases ($\alpha - \beta_0 = \alpha_0 \downarrow$), leading to reductions in both the lift coefficient (C_y^{α} ↓) and drag coefficient (C_x^{α} ↓). This causes a decline in the thrust coefficient ($\overline{\tau}$ ↓) and, subsequently, a reduction in propeller thrust (P↓), as illustrated in Figure 3.

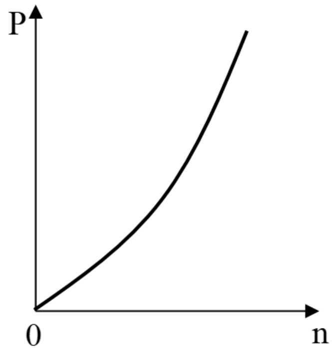

Figure 2. Dependence of Propeller Thrust on Rotational Speed n ($\overline{\tau}$ = const)

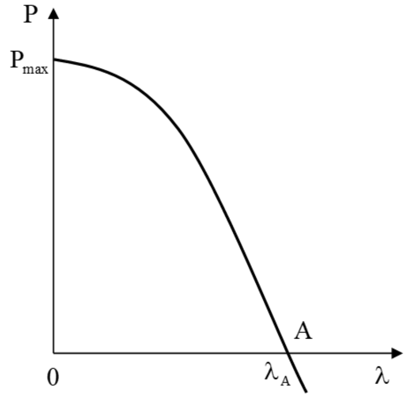

Figure 3. Propeller Thrust Characteristics

From the propeller thrust characteristics graph, the following observations can be made:

- At $\lambda = 0$ (V = 0): This corresponds to the static condition (zero axial velocity) of the propeller. In this mode, the propeller generates maximum thrust (P_{max}), termed the heavy-load propeller mode. However, since no translational work is performed, the propeller efficiency is zero.

- For $0 < \lambda < \lambda_A$: This range represents the propeller's primary operating mode λ_A. Here, the thrust coefficient $\overline{\tau} > 0$. Within this interval, an optimal operating point exists at $\lambda = \lambda_{tu}$, where propeller efficiency reaches its maximum value ($\eta = \eta_{max}$).

- At $\lambda = \lambda_A$: Thrust P becomes zero $(\overline{\tau} = 0)$. The total aerodynamic force acting on the propeller aligns with the rotational plane and equals the rotational resistance force. All input power is consumed to overcome this resistance, resulting in zero useful work and zero efficiency.

- For $\lambda > \lambda_A$: Thrust becomes negative (P < 0), known as the braking mode. This regime is utilized in propeller-driven aircraft for post-landing deceleration or during dives to reduce speed. The angle of attack (α) in this mode is negative.

III. EXPERIMENTAL SETUP FOR PROPELLER THRUST MEASUREMENT

3.1. Airflow Generation System

To simulate real-world operating conditions for aircraft propellers, the experimental setup employs a closed-loop subsonics wind tunnel (OKĐ-0.2M). This wind tunnel generates a stable airflow within the test section, with adjustable airflow velocities ranging from 0 to 0.2 Mach. The schematic of the wind tunnel is illustrated in Figure 4.

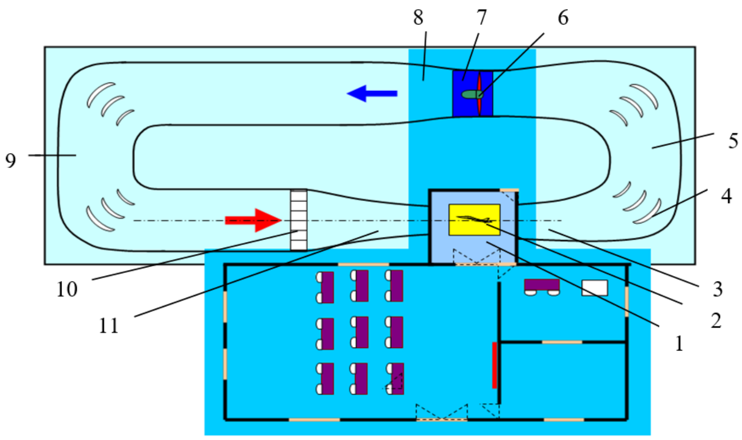

1-Test section
2-Ropeller model
3-Small Diffuser Tube
4-Main Flow Plates
5-Air Recirculation Duct to the Engine
6-Three Phase Electric Fan Motor
7-Engine Compartment
8-Large Diffuser Tube
9-Air Guide Tube
10-Flow Stabilization Device
11-Acceleration Tube

Figure 4. Schematic Diagram of the OKĐ-0.2M Wind Tunnel

3.2. Propeller Model

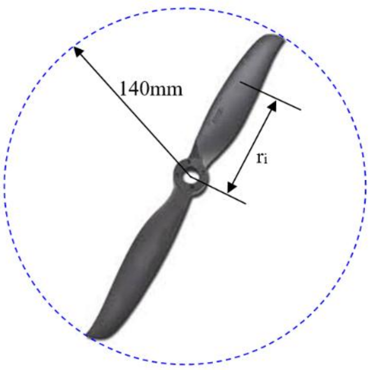

Figure 5. Emp 11x5.5 Propeller

Table 1. Parameters of the Emp 11x5.5 Propeller

Element Radius (r_i, mm)	Profile Chord (b_i, mm)	Profile Pitch Angle (φ_i)
20	22	70
40	30	50
60	28	35
80	26	25
100	20	15
120	15	10
140	-	2

3.3. Functional Diagram of the Propeller Assembly

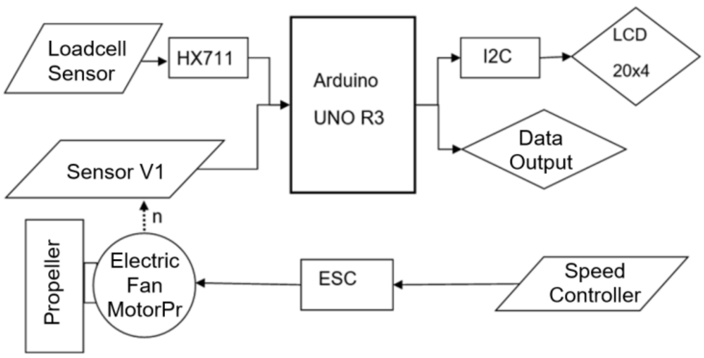

Figure 6. Functional Diagram of the Propeller Assembly

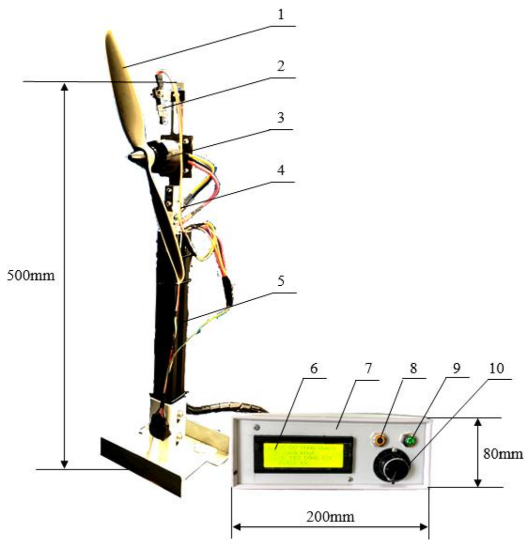

Figure 7. Propeller Assembly

1-Propeller; 2-Propeller rotational speed measurement device; 3-Electric motor; 4-Propeller thrust measurement device; 5-Fixture; 6-Display screen; 7-Control box; 8-Motor power button; 9-5V power button; 10-Control knob

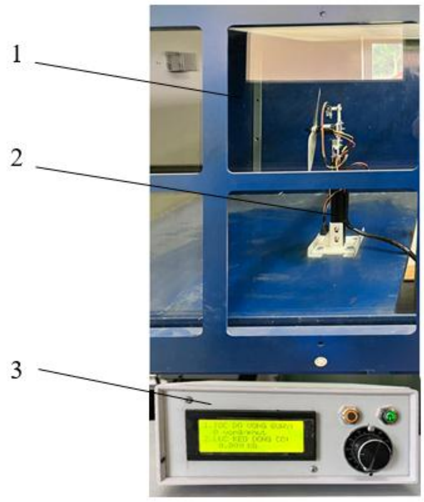

Figure 8. Mounting the Propeller Assembly onto the OKD-0.2M Working Chamber

1- Propeller assembly; 2- Propeller assembly fixing bolt; 3- OKD-0.2M Test section

IV. RESULTS AND DISCUSSION

4.1. Determination of Thrust Dependence on Propeller Rotational Speed

Table 2. Thrust Results with Varying Rotational Speed

No. / Parameter	1	2	3	4	5	6	7	8	9
Rotational speed n (RPM)	2504	3613	4582	5861	6607	7185	8577	8981	10388
Thrust P (kG) (Experimental)	0.097	0.178	0.273	0.446	0.602	0.674	0.766	0.846	1.011
Thrust P (kG) (Theoretical)	0.090	0.189	0.286	0.382	0.581	0.618	0.756	0.847	0.958
Error compared to experiment (%)	7.22	6.18	4.67	14.35	3.49	8.31	1.31	0.12	5.24

4.2. Determination of Thrust Dependence on Airflow Velocity

Table 3. Thrust Results with Varying Airflow Velocity

No. / Parameter	1	2	3	4	5	6	7	8	9
Airflow velocity (m/s)	0	2	4	6	8	10	12	14	17
Thrust P (kG) (Experimental)	0.716	0.664	0.594	0.522	0.415	0.386	0.311	0.218	0.101
Thrust P (kG) (Theoretical)	0.709	0.672	0.622	0.556	0.501	0.422	0.319	0.220	0.078
Error compared to experiment (%)	0.98	1.20	4.71	6.51	20.72	9.33	2.57	0.92	22.77

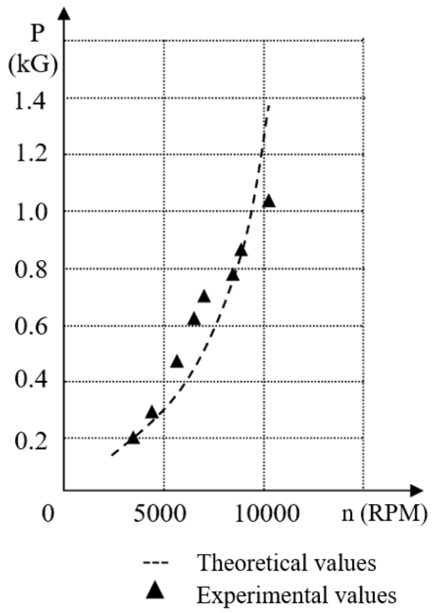

Figure 9. Dependence of Thrust on Propeller Rotational Speed

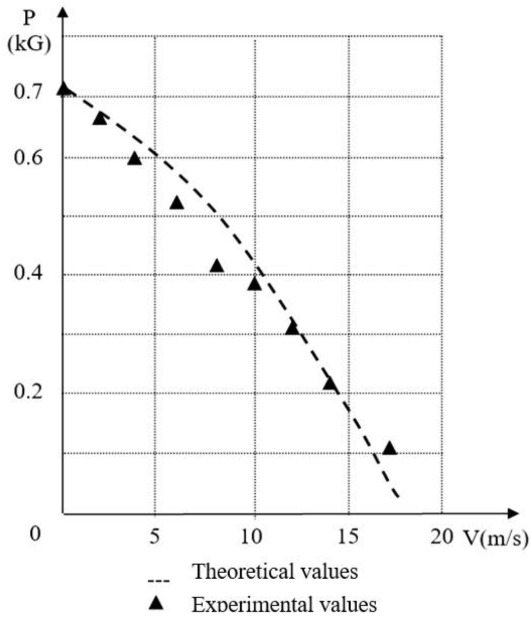

Figure 10. Dependence of Thrust on Airflow Velocity at n=8000RPM

Observations from Figures:

For Figure 9: As the propeller rotational speed (n) increases, the thrust (P) also increases, consistent with theoretical predictions. The error between experimental and theoretical results ranges from 0.12% to 14.35%, indicating a reasonable alignment with the theoretical model. However, experimental thrust values rise more rapidly than theoretical predictions at higher rotational speeds.

For Figure 10: With n = 8000 RPM, as the airflow velocity V increases, the thrust gradually decreases, which reflects the reduction in propeller efficiency as the airflow velocity increases. The theoretical and experimental results both show this decreasing trend, but the decrease in the experimental results is more pronounced than in the theoretical results, especially at high airflow velocities. This may be related to the uneven distribution of airflow across the propeller blades due to the occurrence of aerodynamic phenomena such as turbulence and boundary layer separation, which the theory does not fully account for

IV. CONCLUSION

The study on fixed-pitch propellers demonstrates a clear relationship between thrust, rotational speed, and airflow velocity. Thrust is proportional to the square of propeller rotational speed and inversely proportional to the freestream velocity. As rotational speed increases, thrust rises correspondingly, while higher airflow velocities initially enhance thrust but eventually reduce propeller efficiency beyond a critical threshold. These findings underscore the importance of balancing operational parameters to optimize propeller performance. The results provide a robust foundation for refining propeller designs to achieve maximum efficiency across varying operational conditions, particularly in applications such as gas turbine engines and unmanned aerial vehicles (UAVs). Future research should expand to include aerodynamic factors like air density, altitude, and ambient temperature, which could further improve propeller performance in real-world scenarios.

Conflict of interest

There is no conflict to disclose.

FUTURE DEVELOPMENT

The experiment can be developed to comprehensively investigate the aerodynamic characteristics of helicopter rotor blades: thrust characteristics, power characteristics, and propeller efficiency. To achieve this, a torque sensor should be added to the electric motor shaft to determine the propeller's power and efficiency when varying rotational speed and airflow velocity.

REFERENCES

[1]. Nguyen Huy Hao, "*Propulsion Efficiency of Propellers and Empirical Coefficients for Determining Propeller Efficiency*". Vietnam Maritime University, Hai Phong, 2015.

[2]. Vu Ngoc Hoe, "*Aerodynamics*". Air Defense – Air Force Academy, Hanoi, 2011.

[3]. Brandt J. B., Selig M, "*Propeller Performance Data at Low Reynolds Numbers",* Urbana, USA, 2011.

[4]. Edward Corrigan, Aaron Altman, "*Survey of Small UAV Propulsion System Performance"*, Dayton, Ohio, 2008.